Supercontinuum Generation in Lithium Niobate Ridge Waveguides Fabricated by Proton Exchange and Ion Beam Enhanced Etching *

Bing-Xi Xiang(项炳锡)[1,2†], Lei Wang(王磊)[3†], Yu-Jie Ma(马钰洁)[1,2], Li Yu(余利)[1,2], Huang-Pu Han(韩黄璞)[3], Shuang-Chen Ruan(阮双琛)[1**]

[1]*Shenzhen Key Laboratory of Laser Engineering, College of Optoelectronic Engineering, Shenzhen University, Shenzhen 518060*

[2]*Key Laboratory of Optoelectronic Devices and Systems of Ministry of Education and Guangdong Province, College of Optoelectronic Engineering, Shenzhen University, Shenzhen 518060*

[3]*School of Physics, Shandong University, Jinan 250100*

(Received 3 November 2016)

We report on the fabrication of the 10-mm-long lithium niobate ridge waveguide and its supercontinuum generation at near-visible wavelengths (around 800 nm). The waveguides are fabricated by a combination of MeV copper ion implantation followed by wet etching in a proton exchanged lithium niobate planar waveguide. Using a mode-locked Ti:sapphire laser with a central wavelength of 800 nm, the generated broadest supercontinuum through the ridge waveguides spans 302 nm (at −30 dB points), from 693 to 995 nm. Temporal coherence properties of the supercontinuum are experimentally studied by a Michelson interferometer and the coherence length of the broadest supercontinuum is measured to be 5.2 μm. Our results offer potential for a compact and integrated supercontinuum source for applications including bio-imaging, spectroscopy and optical communication.

PACS: 42.65.Wi, 61.80.Jh, 42.70.Mp, 42.82.Et DOI: 10.1088/0256-307X/34/2/024203

Supercontinuum (SC) generation has received enormous attention over the past decades due to its numerous applications in the generation of optical frequency combs, spectroscopy, frequency metrology, pulse compression and tunable multi-wavelength laser sources.[1−7] Additionally, because of its low absorption and scattering coefficients in tissue and cells, the SC at the near-visible spectral window (around 800 nm) will provide potential applications in bio-imaging,[8−12] such as optical coherence tomography (OCT)[9,10] and coherent anti-Stoke Raman scattering (CARS) microscopy.[11,12] Such SC sources can also be used for all-optical signal processing and quantum optics.[13−15] A photonic crystal fiber has achieved success in SC generation due to its ability to control the dispersion with high precision, which ensures the generation of large bandwidth SC spectra. In recent years, broadband waveguide-based SC sources have attracted much attention, because the waveguide can make supercontinuum sources more robust and compact, lower cost, and with higher nonlinear parameter in comparison with the SC generation from photonic crystal fibers. The waveguide-based SC sources will become important elements in expanding the functionality of integrated optic systems.

Lithium niobate ($LiNbO_3$, LN) is an extensively studied material for integrated optics and nonlinear optics due to its excellent electro-optical piezo-electric nonlinear properties.[18] Moreover, $LiNbO_3$ with balance of wide transparent range of wavelength, large band-gap (3.8 eV)[19] and third-order nonlinear refractive ($n_2 = 1.13 \times 10^{-19}\,m^2/W$ at 800 nm)[20] provides prospective applications in the field of SC generation covering broad spectral region ranging from visible to mid-infrared. $LiNbO_3$ waveguide-based broadband SC generation has been realized in proton-exchanged waveguides.[21−23]

Compared with the conventional proton-exchanged waveguide, the ridge waveguide possesses some attractive properties such as smaller cross section dimensions, higher optical density and smaller bending radii of curved waveguide owing to its large index contrast to the surrounding air, which can enhance the nonlinear effects and the integration level of optical devices.[24−26] Ridge structures in $LiNbO_3$ have been fabricated by several approaches such as wet etching,[25,27] ion beam etching (IBE)[28] and reactive ion etching (RIE).[29,30] Recently the ion beam enhanced etching (IBEE) method on $LiNbO_3$ crystals has attracted great interest because of its advantages of high selectivity, short fabrication times and independence from the crystal orientation.[31−35] Combined with different planar waveguide fabrication technologies, for example, titanium diffusion,[33] ion implantation/irradiation[34] and liquid-phase epitaxy,[35] high-quality ridge waveguides with low loss have been realized. Annealed proton exchanging (APE) is a mature method to fabricate a low-loss waveguide in $LiNbO_3$ crystals.[36] Unfortunately, there has been no investigation on for-

*Supported by the National Natural Science Foundation of China under Grant Nos 61575129 and 11375105, the Postdoctoral Science Foundation of China under Grant No 2016M602511, the Shenzhen Science and Technology Planning under Grant No JCYJ20160422142912923, and the State Key Laboratory of Nuclear Physics and Technology, Peking University.

†They contributed to this work equally.

**Corresponding author. Email: scruan@szu.edu.cn

© 2017 Chinese Physical Society and IOP Publishing Ltd

mation of ridge waveguides on APE $LiNbO_3$ through the IBEE method so far.

In this Letter, we report on the first observation of SC generation in the $LiNbO_3$ ridge waveguides fabricated by APE as well as IBEE etching induced by Cu ion implantation. The mode propagation properties of the ridges are also investigated. The generated broadest SC ranges from 693 to 995 nm when pumping the waveguide at 800 nm. The coherence lengths of SC are measured to characterize the temporal coherence properties by a Michelson interferometer.

The planar $LiNbO_3$ waveguide was formed by the APE method. A pure z-cut $LiNbO_3$ wafer was exchanged in pyrophosphoric acid for 20 min and annealed at 375℃ for 5 h in dry O_2. This process promoted the formation of α-phase planar waveguide. The refractive index profile of a planar waveguide was reconstructed by a computer code based on the i-WKB method.[37]

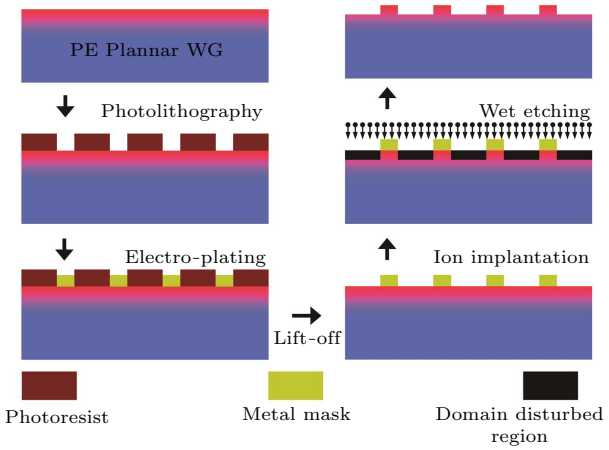

Fig. 1. Fabrication process of the ridge waveguides in the α-phase APE $LiNbO_3$ planar waveguide.

The schematic diagram of the IBEE we carried out is depicted in Fig. 1. Before the photolithography process, the APE samples were cleaned carefully. Then standard photolithography and electro-plating procedures were performed on the samples to form metal (Cu) masks with thickness of 4–5 μm for blocking energetic ions. The opening sections of the sample will be damaged due to the energy deposition process of the implantation, thus these opening parts could be etched by diluted HF etchant and the ridge waveguide structures could be formed. In the next step, 6 MeV Cu ions were implanted into the samples at the fluence of 6×10^{14} ions/cm^2. The ion implantations were carried out by 1.7 MV tandem accelerator at Peking University. The ion beam was scanned electrically to ensure a uniform implantation. Here 7° angle was deviated from the axis of the crystal to avoid the channeling effect. After the implantation, metal patterns were removed and the samples were etched in a 5% HF:H_2O solution. The ultimate etched depth could be controlled by adjusting the etching time and ion energy. The etched morphology of the ridge waveguides was observed using an optical microscope (Olympus BX51M, Japan) and a scanning electron microscope (SEM). The end facets of the samples were polished carefully before the end-face coupling measurement. Laser light was coupled into ridge waveguides by using the microscope objective lens. The polarization of the lasers could be controlled by wave plates. The modal profiles were collected by the charge coupled device (CCD) camera. The modal properties of the ridge waveguides were simulated by the finite difference beam propagation method (FD-BPM). The SRIM2013 program (the stopping and range of ions in matter) was used to simulate the energy deposition process inside the crystal.[38]

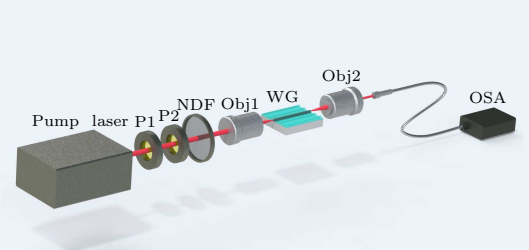

Fig. 2. Experimental setup of SC generation in $LiNbO_3$ ridge waveguides. P1: half-wave plate; P2: polarizer; NDF: neutral density filter; Obj1: objective; WG: $LiNbO_3$ ridge waveguides; Obj2: objective; and OSA: optical spectrum analyzer.

The experimental setup for SC generation in $LiNbO_3$ ridge waveguides is shown in Fig. 2. A mode-locked Ti:sapphire laser (Legend Elite, Coherent) was used as a pump source with a central wavelength of 800 nm. The laser provided pulses with about 35 fs duration, a repetition rate of 1 kHz, and a maximum average output power of 4 W. A half-wave plate (P1), a polarizer (P2) and a variable neutral density filter (NDF) wheel were used to adjust the polarization and peak power of the input pulses. The pulses were coupled into the $LiNbO_3$ ridge waveguides by a 20× objective lens (NA=0.4). The output pulse spectrum was collected by using a 40× objective (NA=0.65) and was recorded by using an Avantes AvaSpec-3648 fiber optic spectrometer. For the temporal coherence property measurement, the SC output from the waveguide was collimated by an objective, and was sent to a Michelson interferometer. One arm of the interferometer could be moved to provide a delay. The power evolution with different delay lengths was recorded by a power meter.

Figure 3 shows the electronic and nuclear energy deposition versus depth of 6 MeV Cu ions implanted into $LiNbO_3$ crystal, which is simulated by SRIM2013. Electronic and nuclear energy depositions determine the implantation profile and the distribution of lattice damage in the $LiNbO_3$ crystal, respectively. The previous investigations about APE $LiNbO_3$ waveguide have shown that the proton concentration in the α-phase region is very low (less than 10%) and the physical and chemical properties of this region are similar to that of the bulk material. We have confirmed that

no evident difference is made to the simulation results after taking proton into account. As shown in Fig. 3, the electronic energy deposition has a maximum value of about 400 eV/Å per ion at the surface and decreases with increasing the depth. The nuclear energy deposition is relatively low in the near surface region and increases to a maximum at a depth of 2.1 μm. Therefore, electronic energy deposition takes the major responsibility for the etching at the surface region[31,33] (surface damage region can be formed when electronic energy deposition exceeds 285 eV/Å per ion[39]), while nuclear energy deposition is the main reason for the etching at the end of the ion tracks.

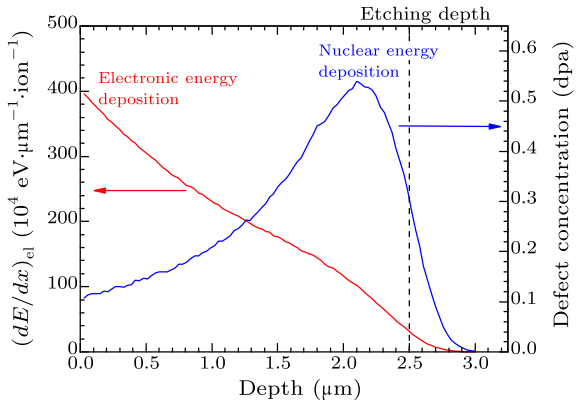

Fig. 3. The energy deposition of 6 MeV Cu ions implanted into $LiNbO_3$ (red line for the electronic energy deposition and blue line for the nuclear energy deposition). The etched depth is also presented in the figure.

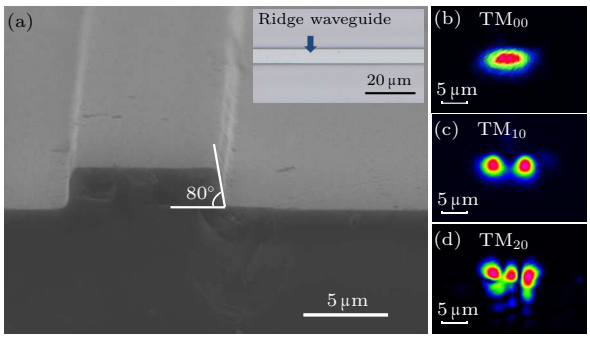

Fig. 4. (a) The SEM picture of the etched ridge structures in the APE planar waveguide. The inset shows the optical microscope image (top view) of the ridge waveguide. The measured intensity distributions of (b) TM_{00} mode, (c) TM_{10} mode and (d) TM_{20} mode in the $LiNbO_3$ ridge waveguide.

Figure 4(a) is the etching results of the APE planar waveguide measured by SEM. The ridge structure with height of 2.5 μm is formed after 40 min etching. Putting the sample in the HF etchant for a longer time (5 h) cannot achieve deeper etching, which indicates that there is a saturation etching depth about 2.5 μm for our $LiNbO_3$ sample. The top side of the ridge waveguide is 8.5 μm wide. The vertical angles of the ridge sidewalls are about 80°. The shape of the fabricated ridge is nearly rectangular. We find that the metal pattern is unchanged after the Cu ion implantation, but swelling after the wet etching process means that the metal mask is not appropriate for recycling in the implantation-etching process. The inset in Fig. 4(a) shows the top view of the ridge waveguide, which is obtained by a metallographic microscope with 1000× magnification using reflected polarized light.

Figures 4(b)–4(d) depict the measured guided modes in the fabricated ridge waveguide at wavelength of 800 nm of the transverse magnetic (TM) mode. It can be obtained that transverse guiding is realized by the present etching process. The etched depth of 2.5 μm is enough for the ridge waveguide formation in our case. Multimode guiding is also observed in the waveguide at wavelength of 800 nm. We measure the propagation loss of the ridge waveguide with the end face coupling method.[40] The propagation loss turns out to be about 1 dB/cm at wavelength of 632.8 nm.

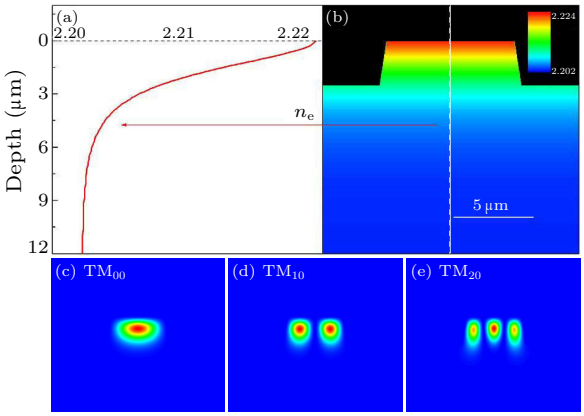

Fig. 5. The reconstructed refractive index profile of (a) APE planar waveguide and (b) ridge waveguide. The simulated intensity distributions of (c) TM_{00} mode, (d) TM_{10} mode and (e) TM_{20} mode in the $LiNbO_3$ ridge waveguide at wavelength of 800 nm.

The dark mode spectra[17] measured by the Model 2010 prism coupling system presented three TM modes at wavelength of 632.8 nm. According to the dark-mode spectroscopy, we reconstruct the n_e profile of the APE planar waveguide through the i-WKB method.[37] Figure 5(a) demonstrates the index profile of the planar waveguide (i.e., the vertical index distribution of the ridge waveguide) at wavelength of 632.8 nm. The simulated refractive index profile of the planar waveguide is a semi-Gaussian curve. By using this 1D profile, we also construct the 2D index mapping (Fig. 5(b)) of the ridge waveguide cross section, the angles of the sidewalls are 80°, which can be deduced from the SEM picture.

Taking the material dispersion into account, the refractive index profile $N_\lambda(x, y)$ of the ridge waveguide at different wavelengths λ can be estimated with[41]

$$N_\lambda(x,y) = N_{\mathrm{sub},\lambda} + \frac{N_{\mathrm{sub},\lambda}}{N_{\mathrm{sub},632.8\,\mathrm{nm}}} \cdot [N_{632.8\,\mathrm{nm}}(x,y) - N_{\mathrm{sub},632.8\,\mathrm{nm}}]. \quad (1)$$

Using the FD-BPM, the mode profiles of TM_{00}, TM_{10}

and TM_{20} modes at 800 nm are calculated, as shown in Figs. 5(c)–5(e), respectively. Multimode guiding behavior is also found in the simulation results at wavelength of 800 nm. Comparing Figs. 4(b)–4(d) with Figs. 5(c)–5(e), we can obtain that there is a reasonable agreement between the experimental and calculated data.

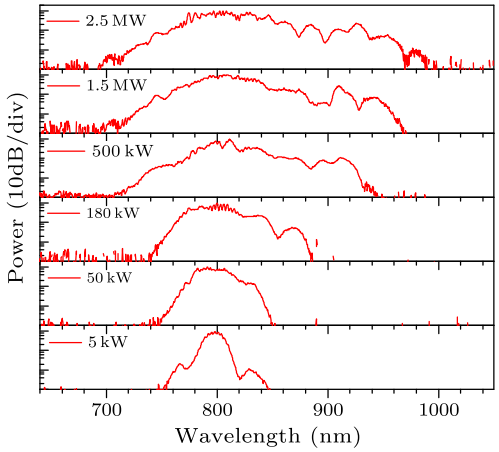

Fig. 6. Evolution of the spectrum as a function of the peak powers coupled into the waveguide.

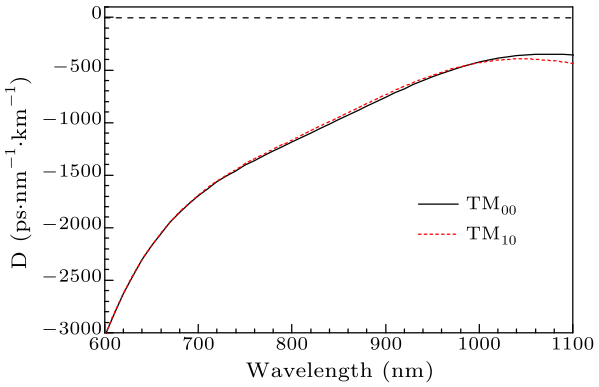

Fig. 7. Dispersion curves of TM_{00} and TM_{10} modes in $LiNbO_3$ ridge waveguide.

The experiment of SC generation in $LiNbO_3$ ridge waveguides is performed using a 35 fs mode-locked Ti:sapphire laser (Legend Elite, Coherent) with a central wavelength of 800 nm. Figure 6 shows the spectra of 800 nm laser pulses after passing through a 10-mm-long $LiNbO_3$ ridge waveguide, as a function of the peak powers coupled into the waveguide. At a low peak power of 5 kW, the shape of the input spectrum is preserved. At 50 kW, small ripples appear in the center of the spectrum, which are mainly attributed to self-phase-modulation (SPM). With increasing the peak power further, the SC spectra broaden continuously. At the available maximal coupled power of 2.5 MW, the −10 dB bandwidth spans 177 nm from 757 to 934 nm and the −30 dB bandwidth spans 302 nm from 693 to 995 nm. The bandwidth can be further broadened by increasing the peak power coupled into the waveguide, while it is limited by the damage occurring at the input facet. The SC power is measured and the throughput is calculated for the SC generation at peak power of 2.5 MW. The SC power is measured by using a silicon photodiode with a measurement range of 200–1100 nm. At this power level, a throughput of 46% is achieved.

The dispersion of the ridge waveguides is calculated by FD-BPM. The effective refractive indices ($n_{\rm eff}$) of TM_{00} and TM_{10} modes at different wavelengths λ can be calculated. The dispersion curves of TM_{00} and TM_{10} modes in the ridge waveguide are depicted in Fig. 7. The results show that the dispersion is normal over the entire concerned range of wavelengths for both TM_{00} and TM_{10} modes. As a result, the primary mechanism for spectral broadening is SPM. The spectra show an obvious asymmetry to longer wavelengths, which indicates that contribution from the Raman scattering effect should also be taken into account.[21,42] Because of the strong positive dispersion in the waveguide, the peak powers reduce rapidly (as a result of quick temporal broadening of the pulse) when the laser pulses pass through the waveguide, which will limit the bandwidth of SC. This can be potentially improved by controlling the waveguide dispersion with better waveguide design. For instance, lithium niobate waveguides in the sub-wavelength size can be fabricated on lithium niobate on insulator (LNOI),[43] which can reduce the peak power and allow for dispersion engineering of the waveguides.

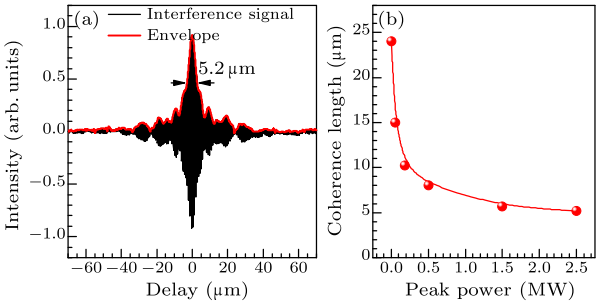

Fig. 8. (a) Interferometric signal and envelope of laser pulses after passing through the $LiNbO_3$ ridge waveguide with the peak power of 2.5 MW. (b) Coherence length as a function of the peak power coupled into the ridge waveguide.

As is widely known, coherence property is a key factor for many applications of SC, such as OCT,[9,10] CARS,[11,12] pulse compression,[6] coherent spectroscopy[44] and wavelength division multiplexing (WDM).[45] To experimentally characterize the coherence property of the generated SC, the coherence lengths of the spectra are measured by a Michelson interferometer. The interferometric signal of the broadest SC is shown together with its envelope in Fig. 8(a). The coherence length of 5.2 μm is determined by measuring the FWHM of the envelope. Figure 8(b) shows the coherence length versus peak powers coupled into the waveguide. As the peak po-

wers are increased, the coherence lengths are shortened. When the peak power reaches its maximum of 2.5 MW, the coherence length reaches the minimum value of 5.2 μm. The shortened coherence lengths of SC output from the ridge waveguide are attributed to the broadened spectra.

In conclusion, we have demonstrated an SC generation in $LiNbO_3$ ridge waveguides pumped at 800 nm. The IBEE with 6 MeV Cu ion implantation is utilized to fabricate ridge waveguides based on the APE $LiNbO_3$ planar waveguide. The etched depth of the ridge structures is about 2.5 μm after 40 min etching. The waveguide property is investigated, showing good guidance at TM polarization. The generated SC spanning 302 nm (at −30 dB points) from 693 to 995 nm in the ridge waveguides has been observed. The coherence length of the broadest SC is measured to be 5.2 μm by a Michelson interferometer. The present results demonstrate that IBEE is an efficient method to fabricate ridge structures in the APE $LiNbO_3$ planar waveguide for coherent SC generation.

References

[1] Dudley J M, Genty G and Coen S 2006 *Rev. Mod. Phys.* **78** 1135
[2] Jiang X, Joly N Y, Finger M A, Babic F, Wong G K L, Travers J C and Russell P St J 2015 *Nat. Photon.* **9** 133
[3] Yan P, Shu J, Ruan S, Zhao J, Zhao J, Du C, Guo C, Wei H and Luo J 2011 *Opt. Express* **19** 4985
[4] Diddams S A, Jones D J, Ye J, Cundiff S T, Hall J L, Ranka J K, Windeler R S, Holzwarth R, Udem T and Hänsch T W 2000 *Phys. Rev. Lett.* **84** 5102
[5] Jones D J, Diddams S A, Ranka J K, Stentz A, Windeler R S, Hall J L and Cundiff S T 2000 *Science* **288** 635
[6] Mollenauer L F, Stolen R H, Gordon J P and Tomlinson W J 1983 *Opt. Lett.* **8** 289
[7] Morioka T, Mori K and Saruwatari M 1993 *Electron. Lett.* **29** 862
[8] Tu H and Boppart S A 2013 *Laser Photon. Rev.* **7** 628
[9] Drexler W, Morgner U, Kartner F X, Pitris C, Boppart S A, Li X D, Ippen E P and Fujimoto J G 1999 *Opt. Lett.* **24** 1221
[10] Morgner U, Drexler W, Kärtner F X, Li X D, Pitris C, Ippen E P and Fujimoto J G 2000 *Opt. Lett.* **25** 111
[11] Mikami H, Shiozawa M, Shirai M and Watanabe K 2015 *Opt. Express* **23** 2872
[12] Xu Q, Shi K and Liu Z 2011 *J. Raman Spectrosc.* **42** 2100
[13] Koyama F 2006 *J. Lightwave Technol.* **24** 4502
[14] Evans C C, Shtyrkova K, Bradley J D B, Reshef O, Ippen E and Mazur E 2013 *Opt. Express* **21** 18582
[15] Hadfield R H 2009 *Nat. Photon.* **3** 696
[16] Dave U D, Uvin S, Kuyken B, Selvaraja S, Leo F and Roelkens G 2013 *Opt. Express* **21** 32032
[17] Xiang B, Ren X, Ruan S, Wang L, Yan P, Han H, Wang M and Yin J 2016 *Sci. Rep.* **6** 31612
[18] Wooten E L, Kissa K M, Yi-Yan A, Murphy E J, Lafaw D A, Hallemeier P F, Maack D, Attanasio D V, Fritz D J, McBrien G J and Bossi D E 2000 *IEEE J. Sel. Top. Quantum Electron.* **6** 69
[19] Dhar A and Mansingh A 1990 *J. Appl. Phys.* **68** 5804
[20] Reddy J N B, Elizabeth S, Bhat H L, Venkatram N and Rao D N 2009 *Opt. Mater.* **31** 1022
[21] Guo H, Zhou B, Steinert M, Setzpfandt F, Pertsch T, Chung H, Chen Y and Bache M 2015 *Opt. Lett.* **40** 629
[22] Phillips C R, Langrock C, Pelc J S, Fejer M M, Jiang J, Fermann M E and Hartl I 2011 *Opt. Lett.* **36** 3912
[23] Langrock C, Fejer M M, Hartl I and Fermann M E 2007 *Opt. Lett.* **32** 2478
[24] Guarino A, Poberaj G, Rezzonico D, Degl'Innocenti R and Gunter P 2007 *Nat. Photon.* **1** 407
[25] Hu H, Ricken R and Sohler W 2010 *Appl. Phys.* B **98** 677
[26] Majkić A, Koechlin M, Poberaj G and Günter P 2008 *Opt. Express* **16** 8769
[27] Hu H, Ricken R, Sohler W and Wehrspohn R B 2007 *IEEE Photon. Technol. Lett.* **19** 417
[28] Rabiei P and Steier W H 2005 *Appl. Phys. Lett.* **86** 161115
[29] Yang W S, Lee H Y, Kim W K and Yoon D H 2005 *Opt. Mater.* **27** 1642
[30] Park W J, Yang W S, Kim W K, Lee H Y, Lim J W, Isshiki M and Yoon D H 2006 *Opt. Mater.* **28** 216
[31] Gischkat T, Hartung H, Schrempel F, Kley E B, Tünnermann A and Wesch W 2009 *Microelectron. Eng.* **86** 910
[32] Schrempel F, Gischkat T, Hartung H, Kley E B and Wesch W 2006 *Nucl. Instrum. Methods Phys. Res. Sect.* B **250** 164
[33] Gill D M, Jacobson D, White C A, Jones C D W, Shi Y, Minford W J and Harris A 2004 *J. Lightwave Technol.* **22** 887
[34] Nicola P D, Sugliani S, Montanari G B, Menin A, Vergani P, Meroni A, Astolfi M, Borsetto M, Consonni G, Longone R, Nubile A, Chiarini M, Bianconi M and Bentini G G 2013 *J. Lightwave Technol.* **31** 1482
[35] Hartung H, Kley E B, Tünnermann A, Gischkat T, Schrempel F and Wesch W 2008 *Opt. Lett.* **33** 2320
[36] Sun J and Xu C Q 2012 *Opt. Lett.* **37** 2028
[37] Chiang K S 1985 *J. Lightwave Technol.* **LT-3 385**
[38] Ziegler J F *Computer Code SRIM* http://www.srim.org
[39] Bianconi M, Bentini G G, Chiarini M, De P, Montanari G B, Menin A, Nubile A and Sugliani S 2010 *Nucl. Instrum. Methods Phys. Res. Sect.* B **268** 3452
[40] Wang L, Chen F, Wang X L, Wang K M, Jiao Y, Wang L L, Li X S, Lu Q M, Ma H J and Nie R 2007 *J. Appl. Phys.* **101** 053112
[41] Wang L, Haunhorst C E, Volk M F, Chen F and Kip D 2015 *Opt. Express* **23** 30188
[42] Psaila N D, Thomson R R, Bookey H T, Shen S, Chiodo N, Osellame R, Cerullo G, Jha A and Kar A K 2007 *Opt. Express* **15** 15776
[43] Poberaj G, Hu H, Sohler W and Gunter P 2012 *Laser Photon. Rev.* **6** 488
[44] Kano H and Hamaguchi H 2003 *Opt. Lett.* **28** 2360
[45] Zeylikovich I, Kartazaev V and Alfano R R 2005 *J. Opt. Soc. Am.* B **22** 1453